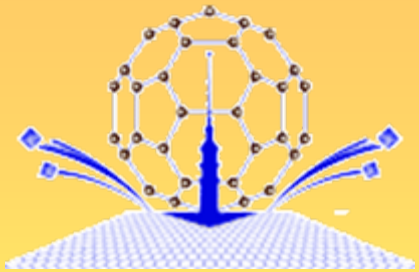

ACN'2011
Conference/School of Young Scientists
" Diagnostics of Carbon Nanostructures "
July 6, 2011, St. Petersburg, Russia

Investigation of Atomic and Electron Structure of Nanocarbon Materials by Use of EXAFS and NEXAFS Spectroscopy Techniques

V.V. Shnitov
Ioffe Institute, 194021, St. Petersburg, Russia
e-mail: v.shnitov@mail.ioffe.ru

Contents

I. Basic Concepts and Definitions

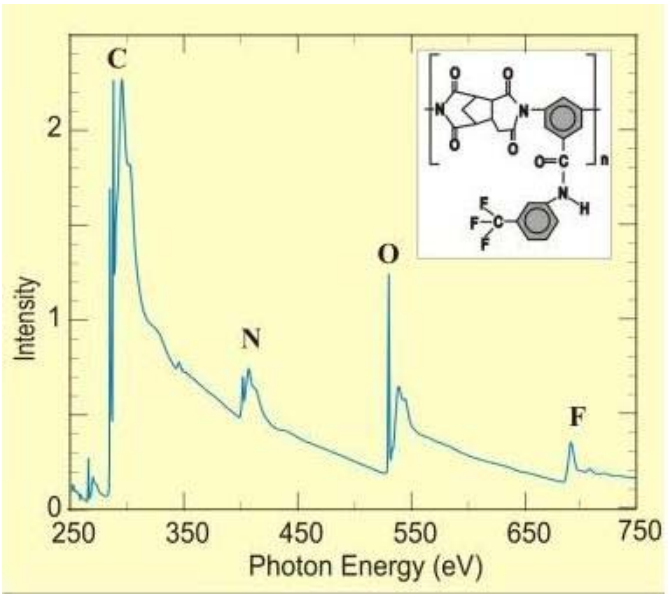

X-ray Absorption Spectroscopy (XAS): Basic Concepts …

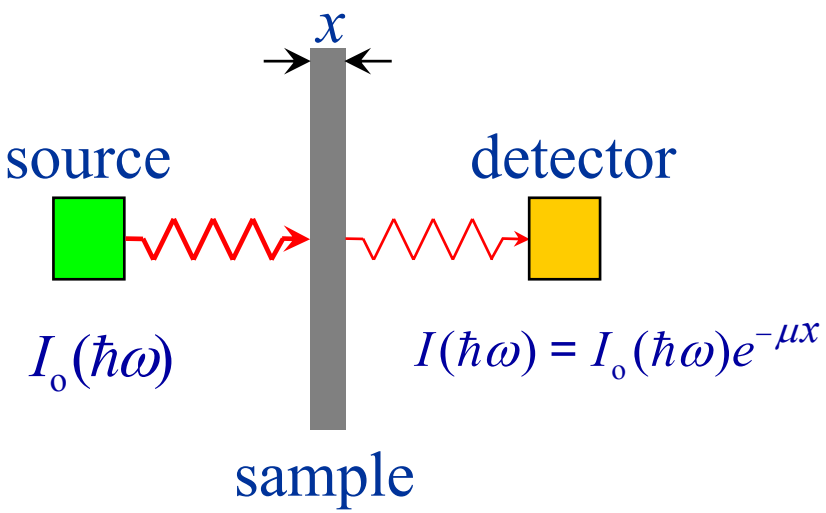

$$\mu(\hbar\omega) \propto \ln\left(I_o / I\right)$$

x-ray absorption coefficient

XAS of a polyimide polymer

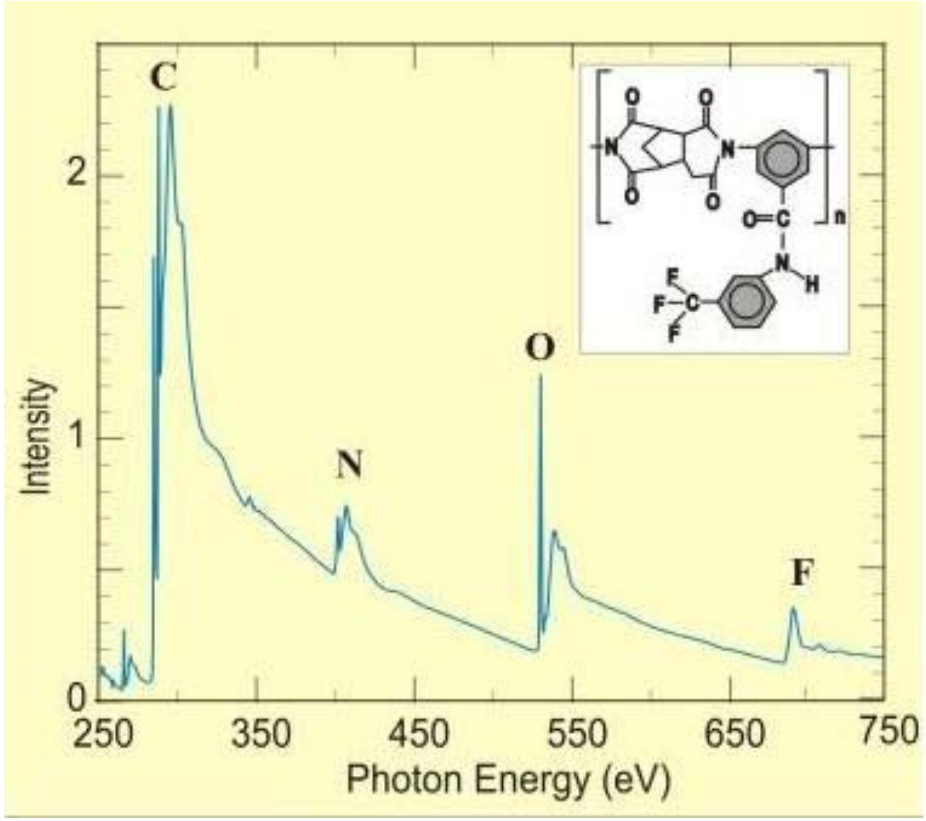

Figure reproduced from the site
http://ssrl.slac.stanford.edu/stohr/nexafs.htm
presenting the book
"J. Stöhr. NEXAFS spectroscopy. Springer, 1996"

…and Basic Definitions

Near Edge X-ray Absorption Fine Structure – NEXAFS

X-ray Absorption Near Edge Structure –XANES

Extended X-ray Absorption Fine Structure – EXAFS

Surface Extended X-ray Absorption Fine Structure – SEXAFS

X-ray Absorption Fine Structure – XAFS

XAS of HOPG

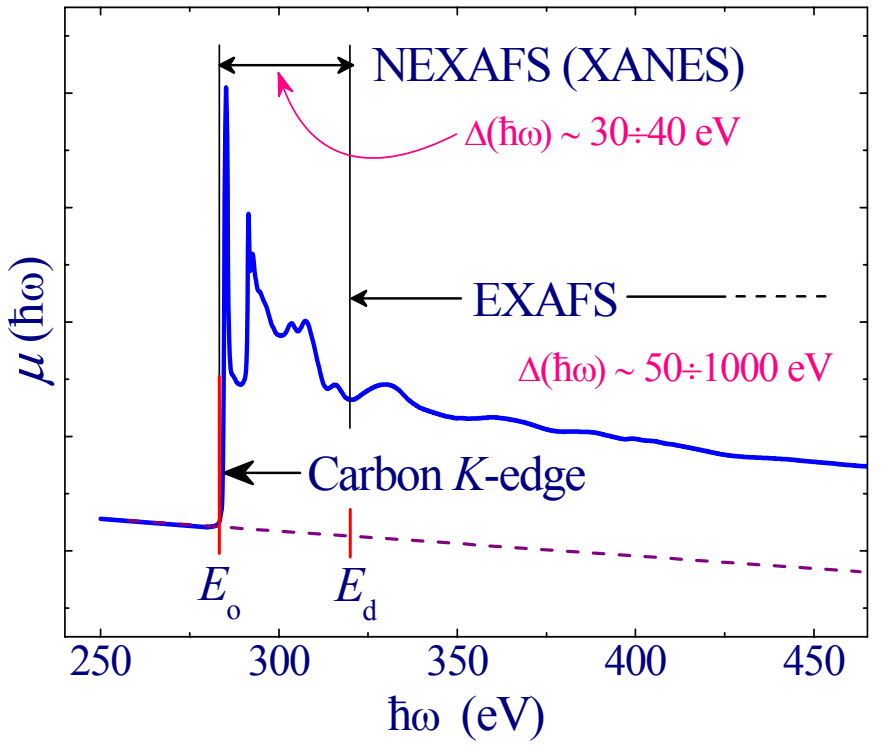

E_o – Carbon K - edge (CK - edge)

$E_o \simeq 285$ eV

E_d – Divide between NEXAFS and EXAFS

$E_d \sim 320$ eV

Important Details of X-ray Absorption Process

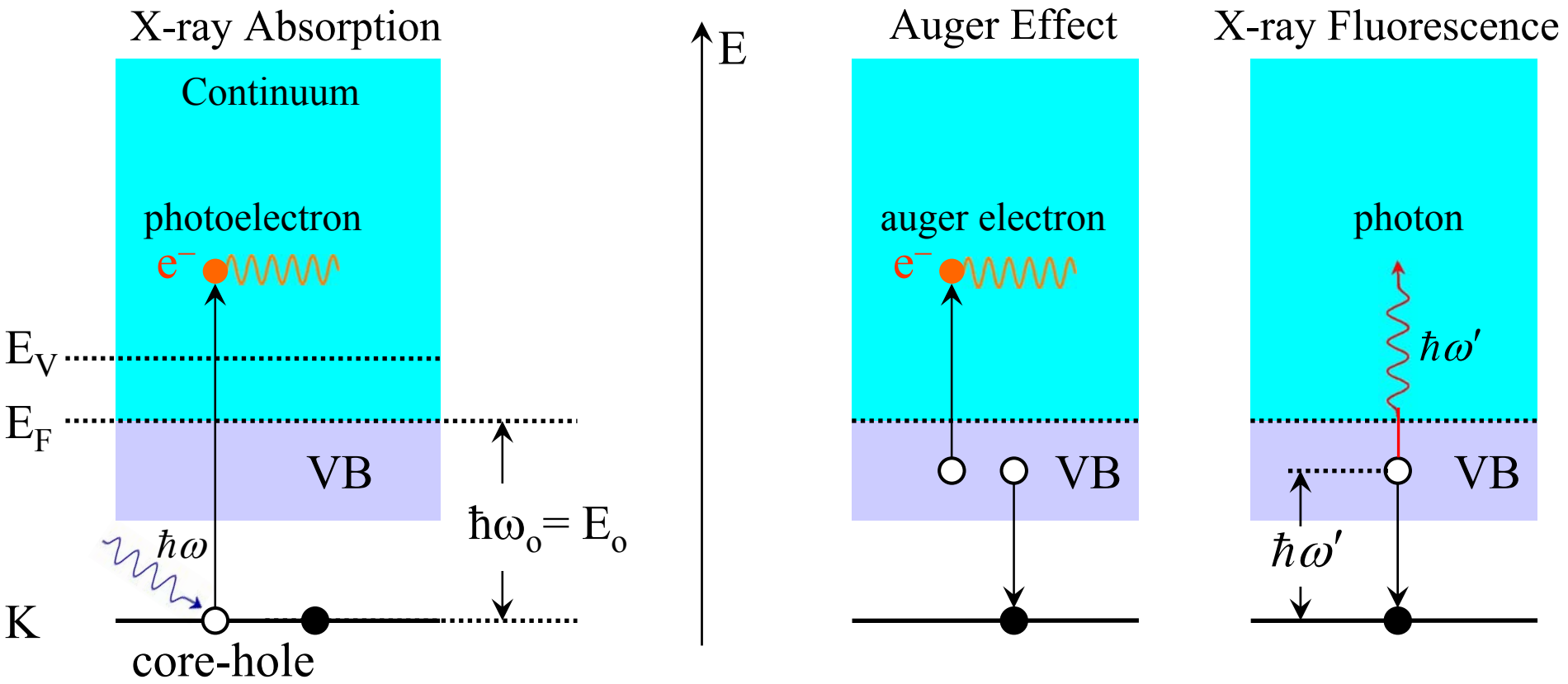

E_o- energy of absorption *K*-edge

τ_h, τ_a, τ_f - total and partials core-hole lifetimes

if $Z \leq 8$ then $\tau_a \sim 10^{-15}$ s $\gg \tau_f \sim 10^{-13}$ s $\Rightarrow$ $1/\tau_h = 1/\tau_a + 1/\tau_f \cong 1/\tau_a \sim 10^{-15}$ s

II. Theoretical Background and a Little of History

$$\chi(k) = S_o^2 \cdot \sum_j \frac{N_j \cdot f_j(k) \cdot e^{-2\sigma_j^2 k^2} \cdot e^{-2R_j/\lambda(k)}}{kR_j^2} \sin\left(2kR_j + \delta_j(k)\right)$$

X-ray Absorption Cross-Section

$$\mu(\hbar\omega) = \sigma_x(\hbar\omega) \cdot n_a$$

σ_x – x-ray absorption cross-section $[\mathrm{cm}^2]$, n_a – atomic density $[\mathrm{atoms} \cdot \mathrm{cm}^{-3}]$

$$\sigma_x\ [\mathrm{nm}^2] = \frac{\text{number of absorbed photons } [\mathrm{s}^{-1}]}{\text{photon flux } [\mathrm{nm}^{-2} \cdot \mathrm{s}^{-1}]}$$

Fermi's Golden Rule $\Rightarrow$ $$\sigma_x(\hbar\omega) \propto \sum_f \left| \left\langle \Psi_f \left| (\mathbf{r} \cdot \mathbf{E}) \right| \Psi_i \right\rangle \right|^2 \cdot \delta(E_f - E_i - \hbar\omega)$$

Ψ_i – initial wave function

localized state with radius $\sim a_B/Z$

Ψ_f – final wave funtion

delocalized state with wave number k and wave length λ

$$\lambda = \frac{2\pi}{k} = \frac{2\pi}{\sqrt{\hbar\omega - E_o}}$$

$(\mathbf{r} \cdot \mathbf{E})$ – dipole transition operator

$\mathbf{E}$ – electric field vector

for K-edges of C, O, N, F the only possible transition $1s \rightarrow 2p$

The Roots of Difference between NEXAFS and EXAFS

NEXAFS
(multiple strong scattering regime)

$$\Psi_f \cong \Psi_f^{(0)} + \Psi_f^{(1)} + \Psi_f^{(2)} + \ldots + \Psi_f^{(n)},\ n \gg 1$$

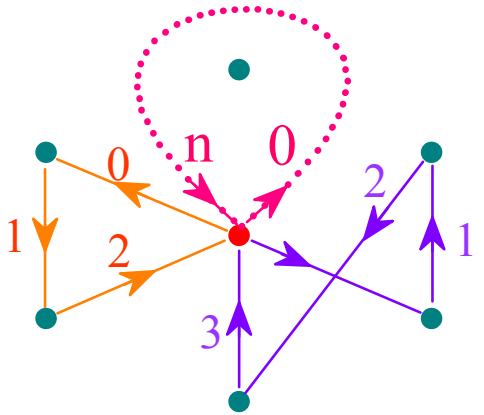

small $k \rightarrow$ large $f(k)$

$\mu(E) \propto \rho(l, E)$

NEXAFS - reflection of l - projected density of unoccupied states $\rho(l, E)$

$$\mu(k) \propto \left| \left\langle \Psi_f \left| (\mathbf{r} \cdot \mathbf{E}) \right| \Psi_i \right\rangle \right|^2$$

$f(k, \theta)$ – elastic scattering amplitude

EXAFS
(single weak scattering regime)

$$\Psi_f \cong \Psi_f^{(0)} + \Psi_f^{(1)}$$

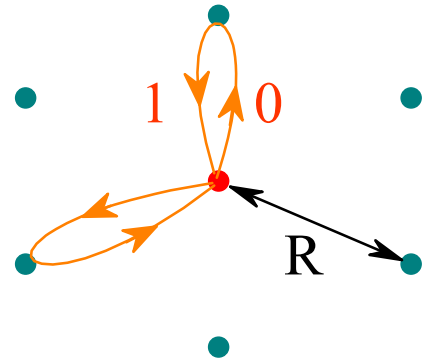

large $k \rightarrow$ small $f(k)$

$\mu(k) \sim f(k) \cdot \sin(2kR)$

EXAFS - reflection of interference pattern traced along photoelectron wave number scale

NEXAFS Dependence on X-Ray Polarization

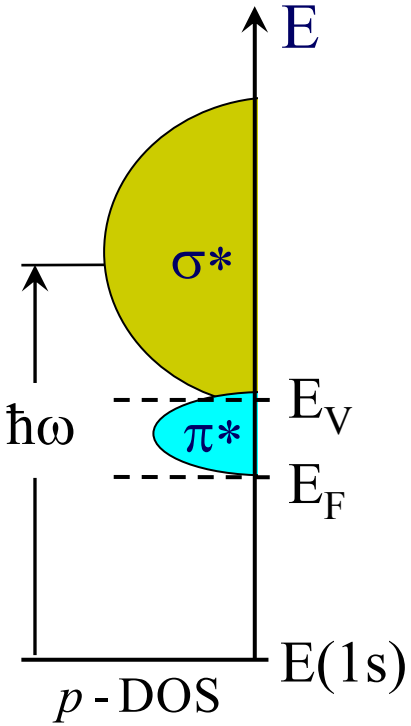

$(\mathbf{r}\cdot\mathbf{E})$

↓

$\mu(E) \rightarrow \mu(\theta, E)$

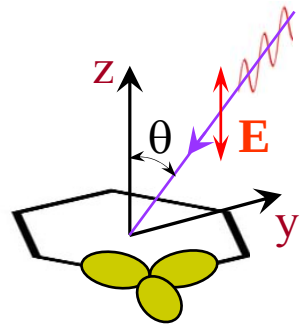

in-plane σ*- orbitals

$\left|\langle \sigma^* | \mathbf{r}\cdot\mathbf{E} | s \rangle\right|^2 \sim \cos^2\theta$

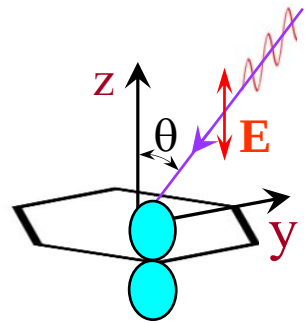

out-of-plane π*- orbitals

$\left|\langle \pi^* | \mathbf{r}\cdot\mathbf{E} | s \rangle\right|^2 \sim \sin^2\theta$

$\mu(\theta, E) \sim \rho_\pi(E)\cdot\sin^2\theta + \rho_\sigma(E)\cdot\cos^2\theta$

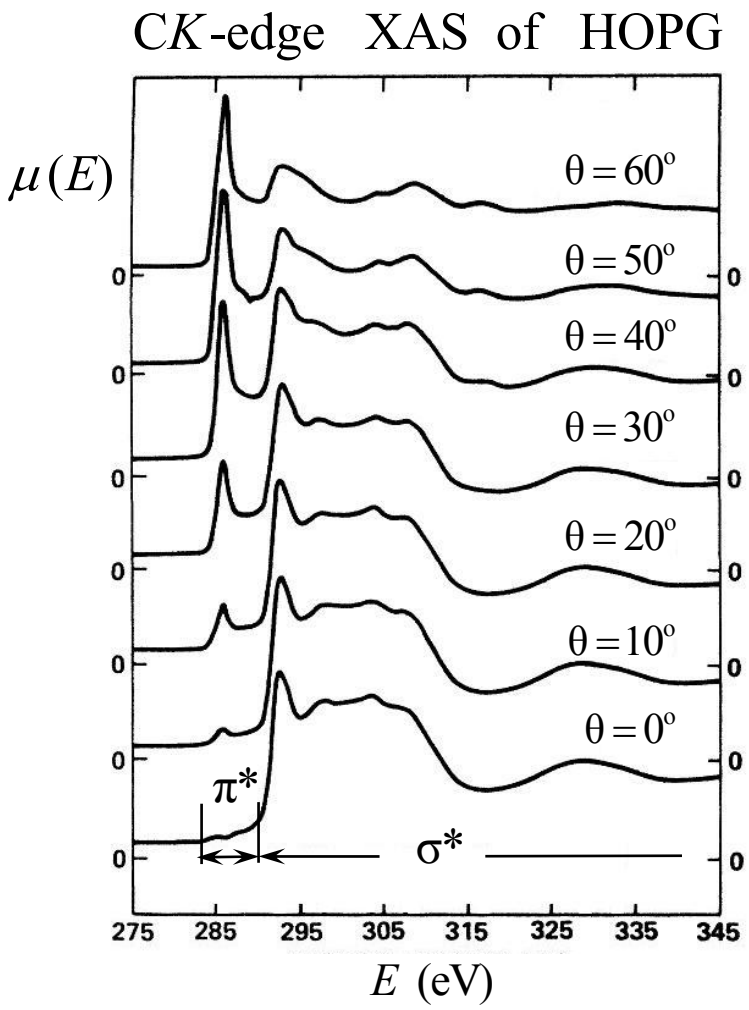

the figure reproduced from
R.A. Rosenberg et al..
Phys. Rev. B **33,** 4034 (1986).

Main features of CK-edge NEXAFS

1. π* - resonances (exciton-like) : $E_F < E_{\pi^*} < E_V$

$E_V = E_F + e\varphi$

for HOPG: $E_V = E_F + 4.7$ eV

2. σ^*_{ex} - core hole (Frenkel) excitons:

$E_V + 1\ \text{eV} < E_{ex} < E_V + 3\ \text{eV}$

for HOPG: $E_{ex} = 291.65$ eV

3. σ* - resonances : $E_V + 3\ \text{eV} < E_{\sigma^*} < E_{EXAFS}$

E_{EXAFS} - lower boundary of EXAFS regime

for HOPG: $E_{EXAFS} \simeq E_F + 30$ eV

NEXAFS reflects: x-ray polarization dependent, core hole-perturbed partial density of unoccupied states (p-DOS) localized within a few atomic sites from the excited atom (R ~ 5 angstrems) [*].

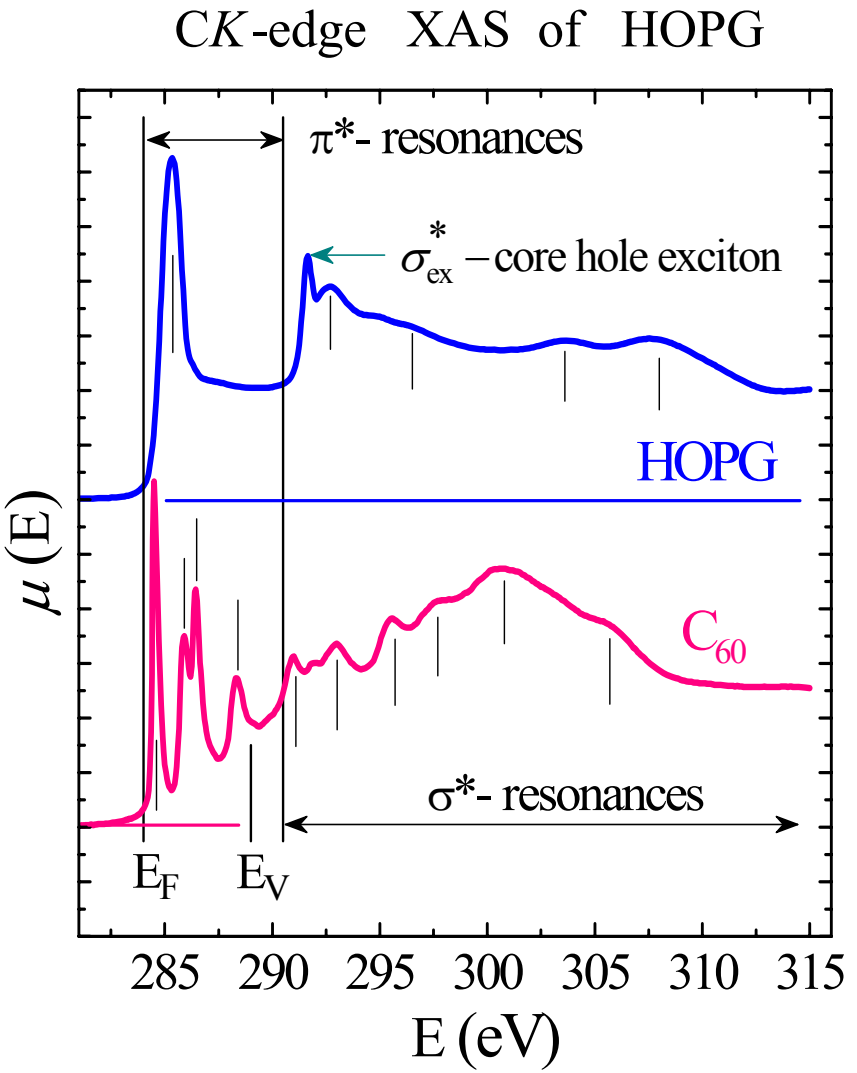

[*] J. Schiessling et al.. J. Phys.: Condens. Matter **15**, 6563 (2003).

Isolation of the Fine-Structure Oscillations $\chi(k)$

XAFS $\mu_o(E)$ for FeO [*]

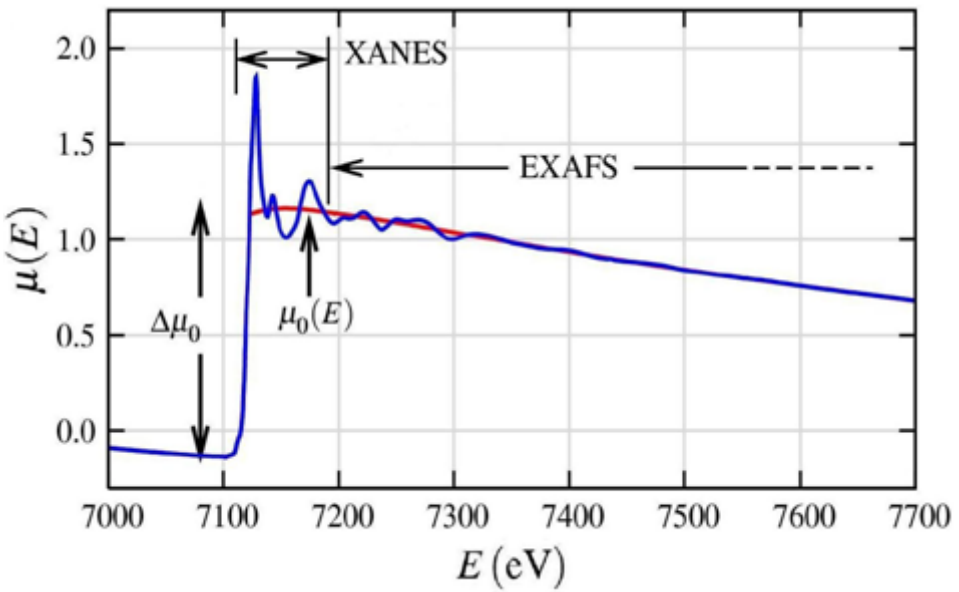

Isolated XAFS $\chi(k)$ for FeO [*]

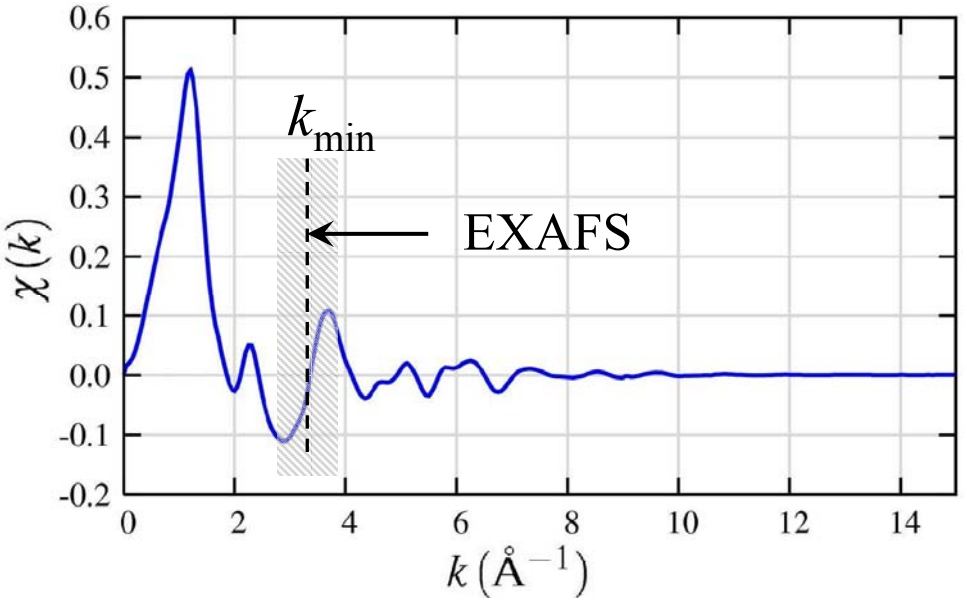

$$\chi(E) = \frac{\mu(E) - \mu_o(E)}{\Delta\mu} \rightarrow k = \sqrt{\frac{2m(E - E_o)}{\hbar^2}} \rightarrow \chi(k) = \frac{\mu(k) - \mu_o(k)}{\Delta\mu}$$

$\mu_o(E)$ - absorption in the absence of neighboring scatterers (atomic-like background)

k_m – lower EXAFS boundary

$$|\chi(k < k_{min})| \gg |\chi(k > k_{min})|$$

[*] M. Newville. Fundamentals of XAFS. University of Chicago, 2004.

EXAFS as a Quantum Interference Phenomenon

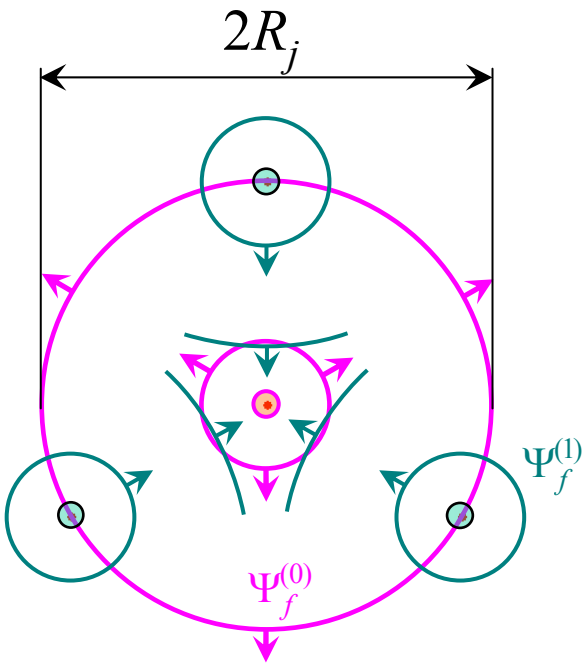

$$\chi(k) \propto \overbrace{\left|\left\langle \Psi_f \left| (\mathbf{r}\cdot\mathbf{E}) \right| \Psi_i \right\rangle\right|^2}^{\mu(\mathrm{k})} - \overbrace{\left|\left\langle \Psi_f^{(0)} \left| (\mathbf{r}\cdot\mathbf{E}) \right| \Psi_i \right\rangle\right|^2}^{\mu_0(\mathrm{k})}$$

Single Scattering Model

$$\chi(k) = \sum_j \frac{N_j \cdot f_j(k)}{kR_j^2} \cdot \sin\left(2kR_j + \delta_j(k)\right)$$

where N_j, R_j are coordination number and avarege distance to atoms in shall j

$$\Psi_f = \Psi_f^{(0)} + \Psi_f^{(1)}$$

$\Psi_f^{(0)}$ – outgoing wave, $\Psi_f^{(1)}$ – backscattered wave

$$\Psi_f^{(0)} \propto \frac{e^{ikr}}{r}, \qquad \Psi_f^{(1)} \propto f(k,\pi)\frac{e^{i(kr+2\delta(k))}}{r}$$

$f(k,\pi)$ – backscattering amplitude

$\delta(k)$ – phase shift

$k_{\min} = \dfrac{2\pi}{R}$ – lower EXAFS boundary

if $R = 1.42$ Å then $k_d \cong 4.5$ Å^{-1}

Taking into Account Many-body Effects

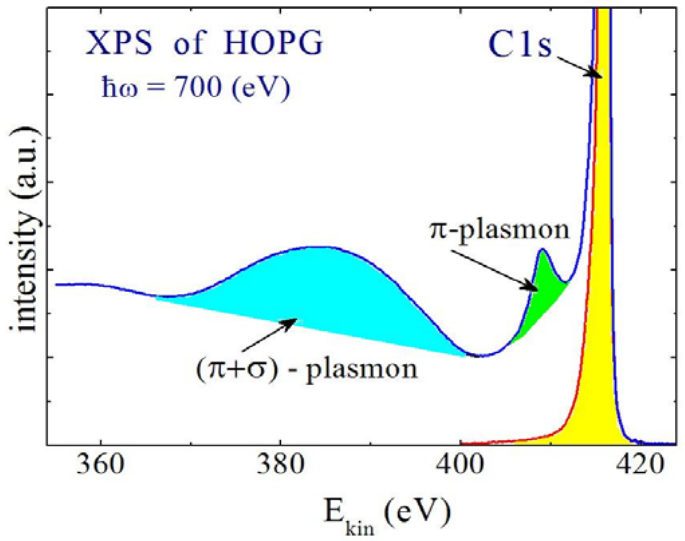

Intrinsic Losses $\rightarrow S_o^2$

(shake-up and shake-off processes)

S_o^2 – amplitude reduction factor;

Structural and Temperature Disorder $\rightarrow e^{-2\sigma_j^2 k^2}$

$e^{-2\sigma_j^2 k^2}$ – Debye-Waller factor

σ_j^2 – mean square displasment of shall j atoms

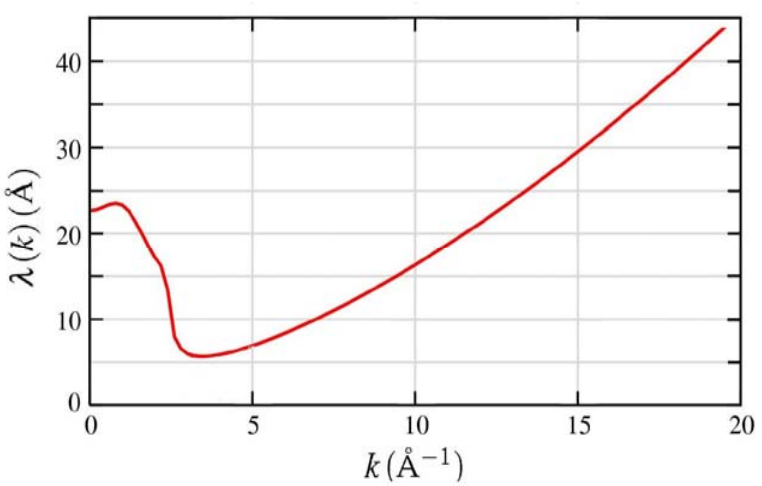

Extrinsic Losses $\rightarrow e^{-2R_j/\lambda(k)}$

$\lambda(k)$ – photoelectron mean free path determined by inelastic scatterings and finite core-hole lifetime

$$\chi(k) = S_o^2 \cdot \sum_j \frac{N_j \cdot f_j(k) \cdot e^{-2\sigma_j^2 k^2} \cdot e^{-2R_j/\lambda(k)}}{kR_j^2} \sin\left(2kR_j + \delta_j(k)\right)$$

The figure reproduced from M. Newville.
Fundamentals of XAFS. University of Chicago, 2004.

Extraction of Structural Parameters from $\chi(k)$ - function

Radial structure function $F(R)$ can be obtained using Fourier transformation of $k\chi(k)$ [*]:

$$F(R) = \int_{k_{min}}^{k_{max}} dk(k\chi(k)) \cdot \sin(2kR)$$

k_{min} and k_{max} are determined, respectively, by lower EXAFS boundary and by acceptable value of signal/noise ratio

for carbon materials:

$k_{min} \simeq 4$ A^{-1} and $k_{max} \simeq 11 \div 12$ A^{-1}

FEFFx (FEFF6 → FEFF8)

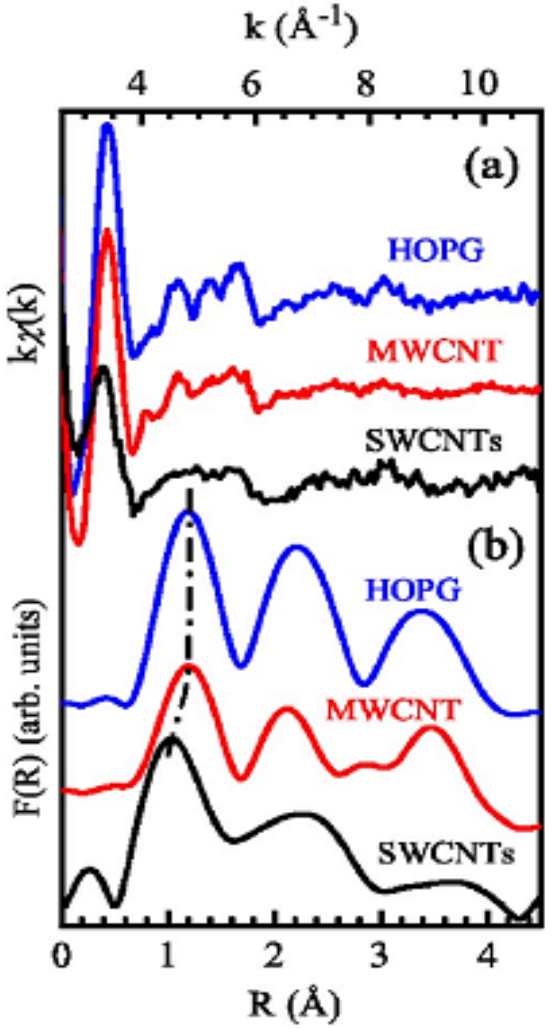

[*]- D. E. Sayers,, E. A. Stern, and F. W. Lytle, Phys. Rev. Lett. **27**, 1204 (1971).

The figures reproduced from P. Castrucci et al. Phys. Rev. B **75**, 035420 (2007).

The Key Points of NEXAFS/EXAFS History

Discovery of X-Rays - Röntgen (1895)

First measurements of absorption edge – Maurice de Brogelie (1913)

The first observation of the fine structure – Fricke (K-edges) (1920), Hertz (L-edges) (1920)

The first theory of NEXAFS ("Kossel structure") and EXAFS ("Kronig Structure") –

Kossel (1920), R. Kronig (1931)

Improvement of theoretical models and experimental facilities (1930s – 1960s)

Creation of valid shot-range-order theory of EXAFS – D. Sayers, E. Stern, F. Lytle (1968-1971)

Appearance of the name EXAFS - F. Lytle, J. Prins (1968)

The dawn of "Synchrotron Era" – (1970s)

Appearance of the names XANES/NEXAFS - A. Bianconi (1980)/J. Stöhr(1982)

Development of highly quantitative multiple-scattering theories of XAFS – (1980s - present time)

III. Some Aspects of Modern XAFS Experiments and XAFS Data Processing Technique

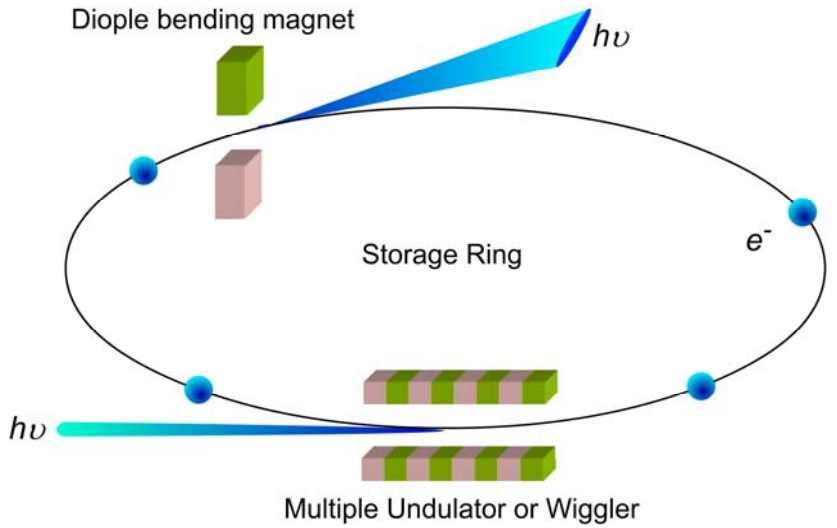

Storage Ring as a X-ray Source

Storage Ring Scheme

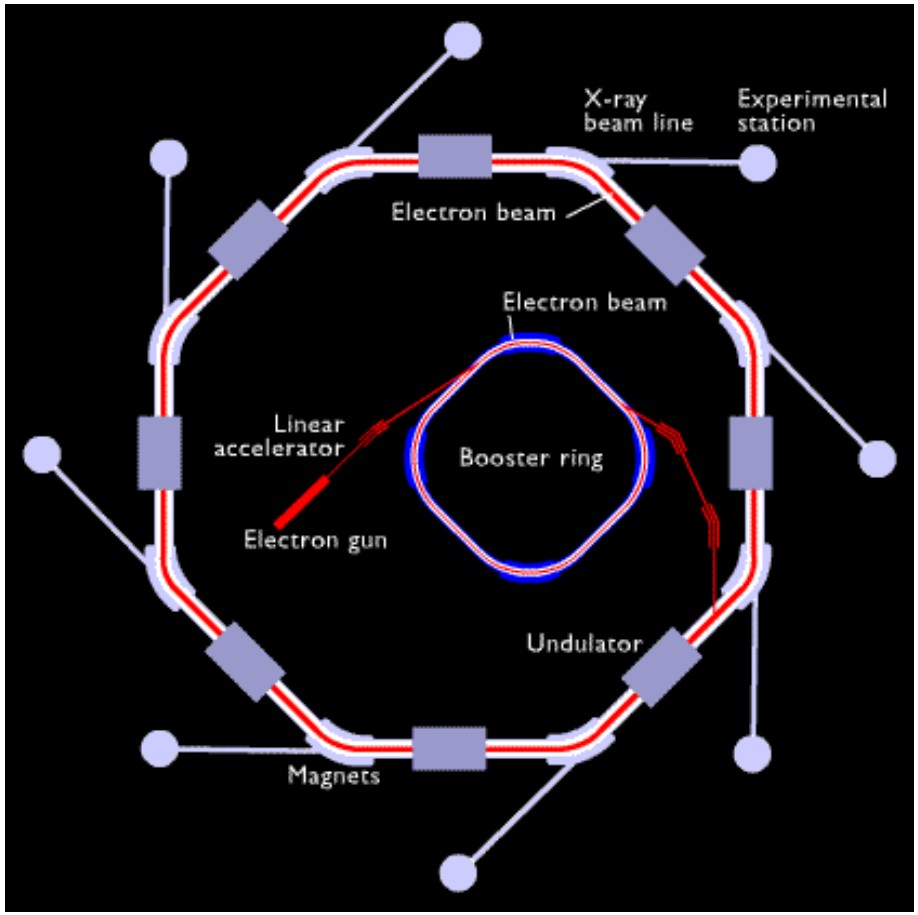

The figure taken from site:
http://www.odec.ca/projects/2005/shar5a0/
public_html/images /model_animated.gif

Synchrotron's Characteristics:

Electron beam energy : E_e [GeV]

Current: i_e [mA]

Circumference: L [m]

Pulse duration (FWHM): τ (ps)

Bending Magnet Field : B [T]

Critical Photon Energy : E_C [keV]

Total Photon Flux: F [photons/s]

$$L = 2\pi R$$

$$E_C = \hbar\omega_C = 0.665 \cdot E_e^2 \cdot B$$

$$F \cong 1.3 \cdot 10^{17} \cdot i_e \cdot E_e$$

Main Characteristic of Synchroton Radiation

Advanced Light Source (ALS).
Berkeley. USA

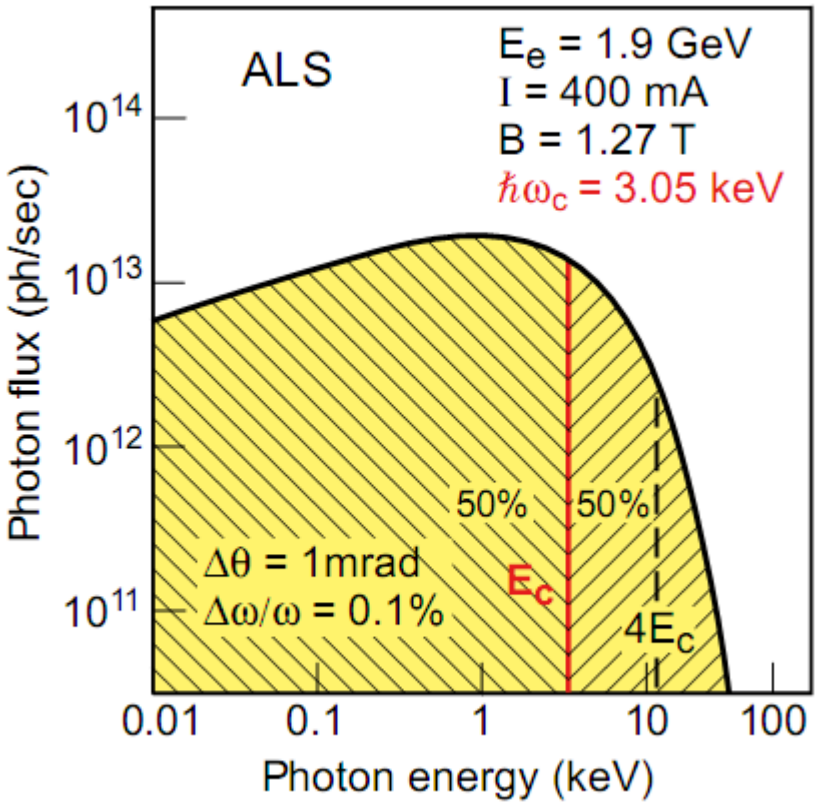

The figure taken from prof. D. Attwood lecture
" Intro to Synchrotron Radiation" EE290F, 16 Jan 2007.
Berkeley. USA.

Dipole Synchrotron Radiation (SR)

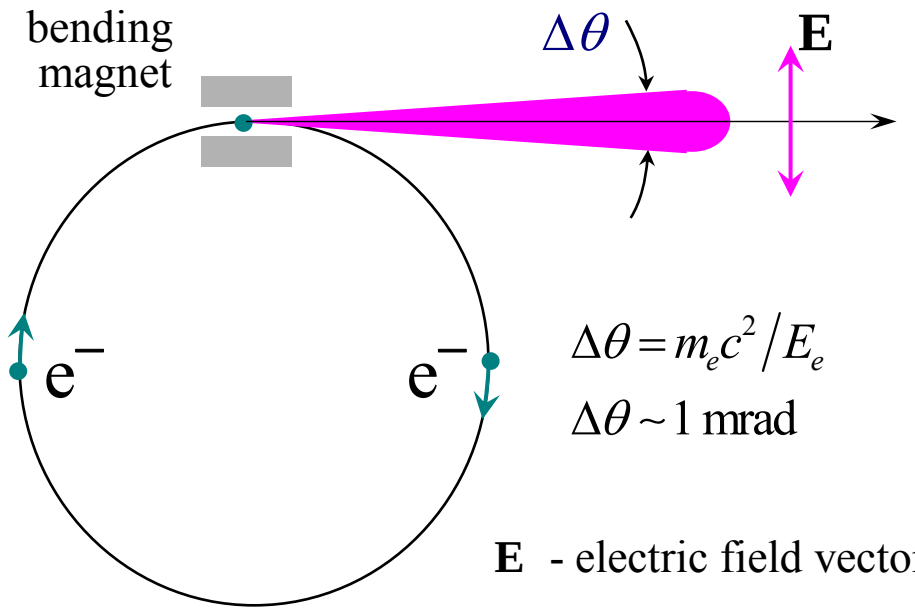

E - electric field vector

1. linear polarization of **E** (in the plane of e^- orbit)

2. extrimely high brightness ($\sim 10^{10}$ brighter than the most powerful laboratory source)

Monochromatization of Synchrotron Radiation

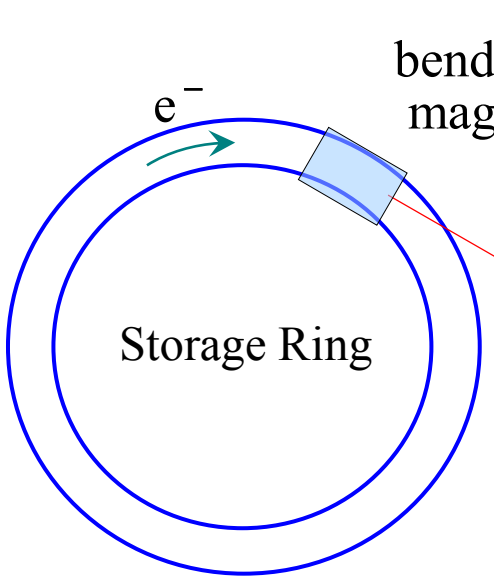

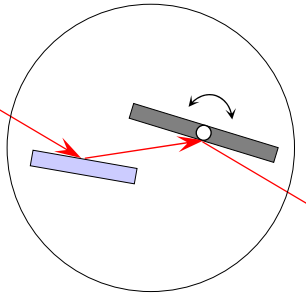

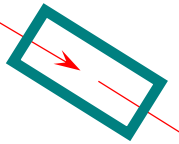

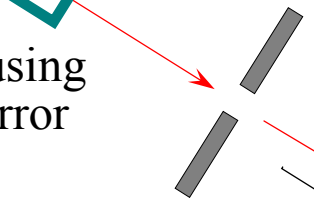

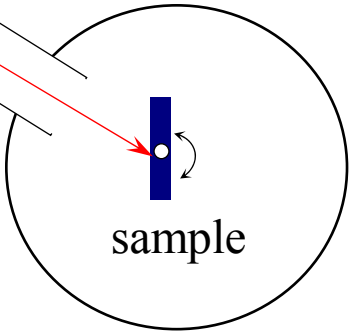

high vacuum analytical chamber

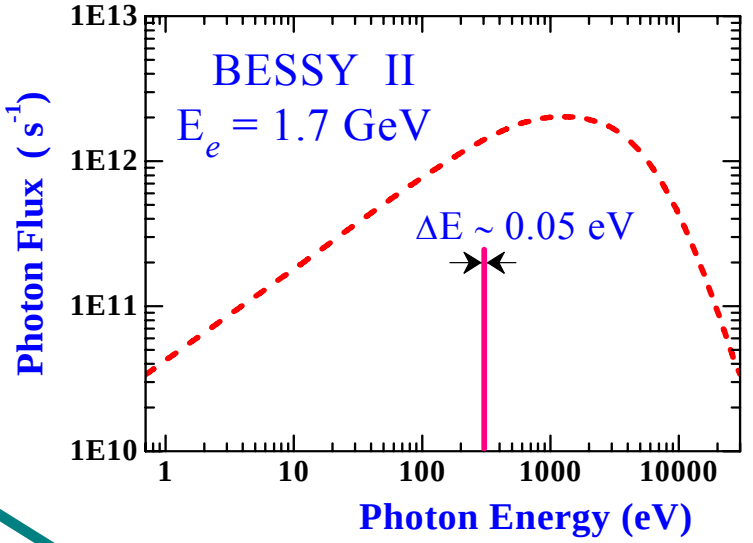

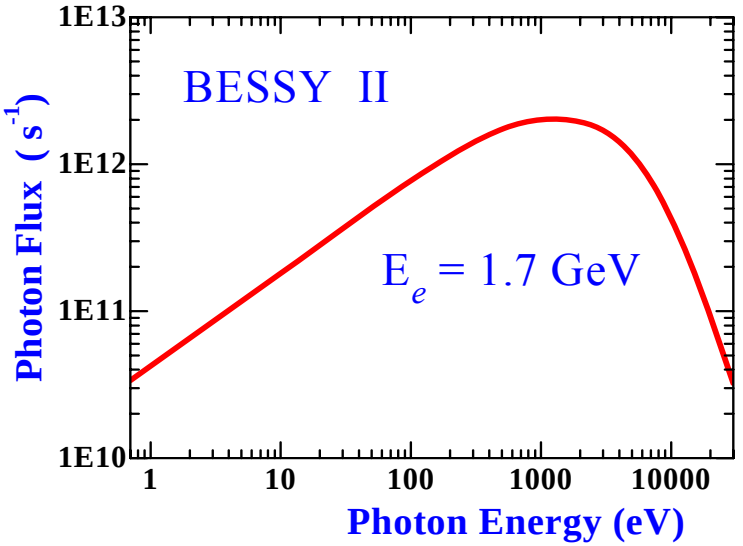

$R = E/\Delta E \sim 10^4$

Energy resolution R is determined by PGM design and exit slit width

Typical Parameters of Third Generation Synchrotrons

Facility	ALS	BESSY II	ESRF	SPring-8
Country	USA	Germany	France	Japan
Electron energy	1.90 GeV	1.70 GeV	6.04 GeV	8.00 GeV
Current (mA)	400	200	300	100
Circumference (m)	197	240	884	1440
RF frequency (MHz)	500	500	352	509
Pulse duration (FWHM) (ps)	35-70	20-50	70	120
Bending magnet field (T)	1.27	1.30	0.806	0.679
Critical photon energy (keV)	3.05	2.50	19.6	28.9
Bending magnet sources	24	32	32	23

The Table taken from prof. D. Attwood lecture " Intro to Synchrotron Radiation" EE290F, 16 Jan 2007. Berkeley. USA.

Recording of the XAS in the Reflection Mode

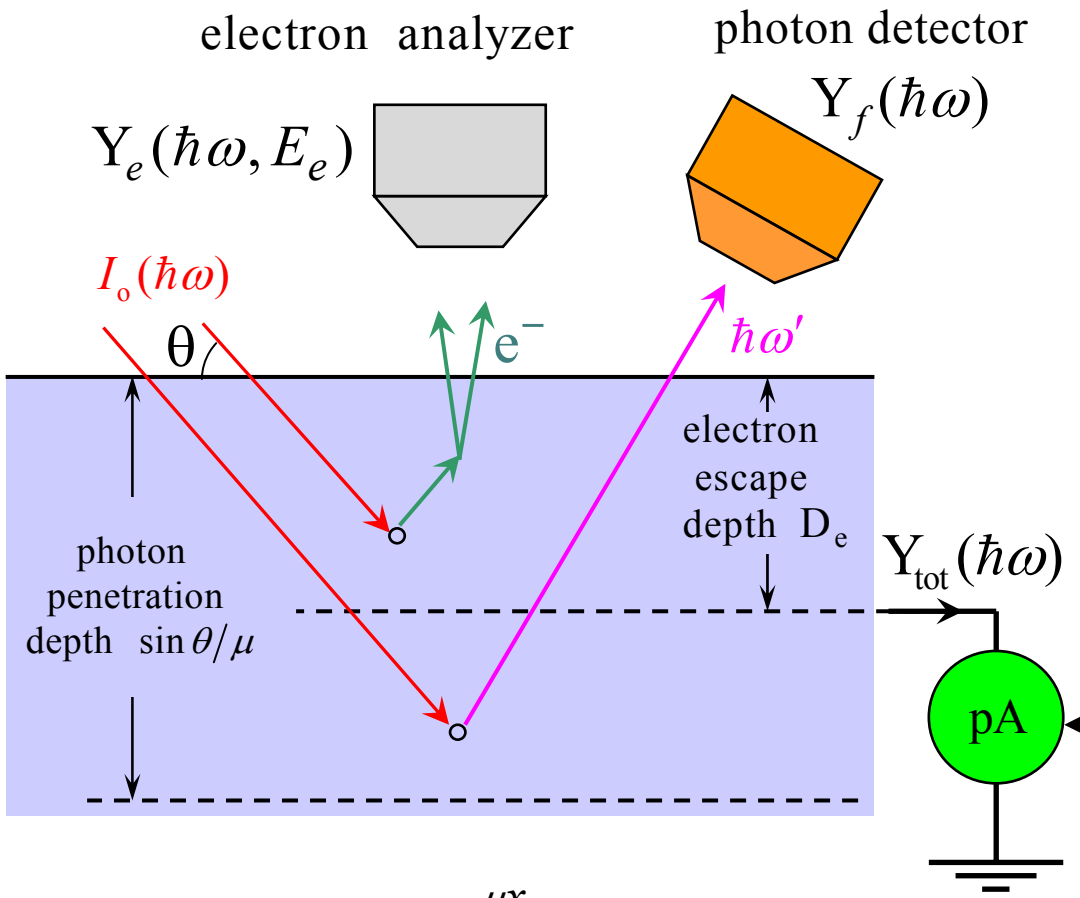

$$I_{abs}(\hbar\omega) \propto Y_e(\hbar\omega) \propto Y_f(\hbar\omega)$$

$Y_f(\hbar\omega)$ – fluorecence yeild (FY)

$Y_e(\hbar\omega)$ – electron yeild (EY)

$$D_e \ll D_f \sim 1/\mu(\hbar\omega')$$

if $Z \le 16$ $\quad Y_f(\hbar\omega) \ll Y_e(\hbar\omega)$

$$Y_{tot}(\hbar\omega) = Y_e(\hbar\omega,\ 0 \le E_e \le \hbar\omega - e\varphi)$$

$$I = I_o\, e^{-\mu x}$$

$$\mu D_e/\sin\theta \ll 1 \quad \Rightarrow \quad I_{abs} = I - I_o \propto \mu \cdot I_o$$

TEY - Total Electron Yield

TFY - Total Fluorecence Yield

Peculiarities of Different Electron Yield Techniques

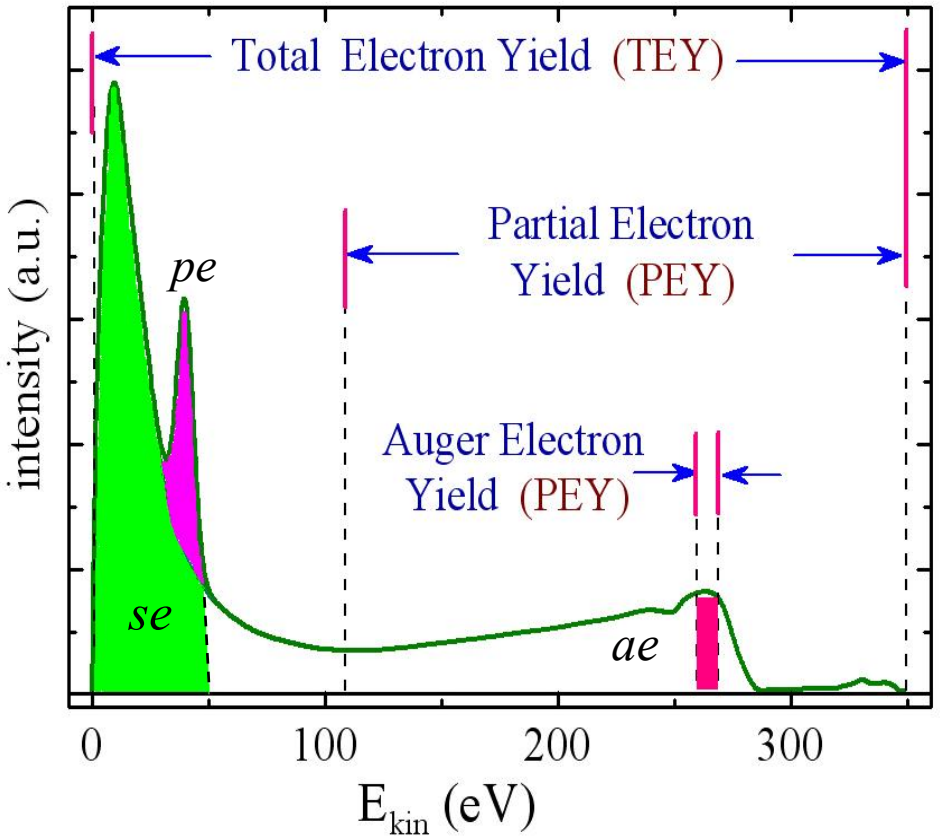

e^- escape depth D_e = XAS information depth

1. TEY: $\mu(\hbar\omega) \propto Y_{tot}(\hbar\omega)/I_o \rightarrow D_e \simeq 50$ Å

2. PEY: $\mu(\hbar\omega) \propto Y_{part}(\hbar\omega)/I_o \rightarrow 10\ \text{Å} \le D_e \le 50$ Å

3. AEY: $\mu(\hbar\omega) \propto Y_{ae}(\hbar\omega)/I_o \rightarrow D_e \sim 10$ Å

Choice of XAS recording mode determines its information depth

se, pe, ae – secondary, photo and auger electrons.

$$Y_{tot} = Y_{se} + Y_{ae} + Y_{pe} \gg Y_{ae} + Y_{pe}$$

TEY - Surface + Bulk

TFY - Bulk

Normalization and Background Correction of the XAS

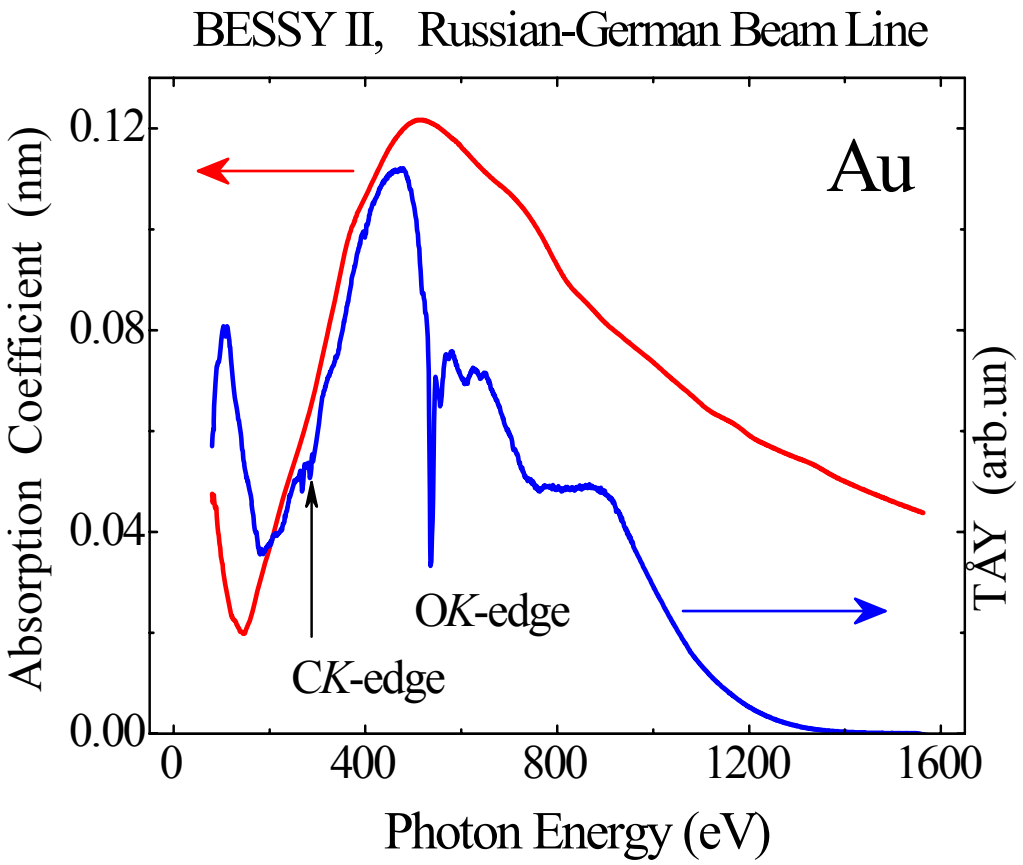

Measured electron yeild $Y_e(\hbar\omega)$ must be corrected for beam line transmission function $T(\hbar\omega)$

$$\mu(\hbar\omega, \mathrm{Au}) = T(\hbar\omega) \cdot Y_e(\hbar\omega, \mathrm{Au})$$

$$T(\hbar\omega) = \frac{\mu(\hbar\omega, \mathrm{Au})}{Y_e(\hbar\omega, \mathrm{Au})}$$

for CK-edge NEXAFS

$$\mu(\hbar\omega, \mathrm{Au}) \simeq \mathrm{const}$$

$$I_o(\hbar\omega) \neq \mathrm{const}$$

$$\mu(\hbar\omega, \mathrm{X}) = \frac{Y_e(\hbar\omega, \mathrm{X})}{Y_e(\hbar\omega, \mathrm{Au})}$$

Normalization and Background Correction of the XAS

Normalization requires reference monitor

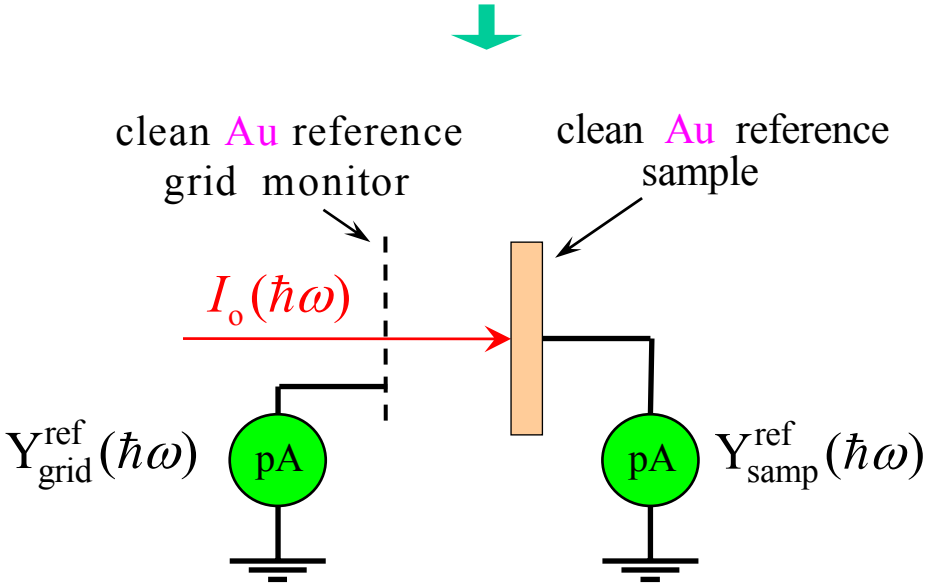

$Y^{ref}_{samp}(\hbar\omega)$ – more simple and controllable

$Y^{ref}_{grid}(\hbar\omega)$ – accounts for photon flux instabilities

BESSY II, Russian-German Beam Line (RGBL)

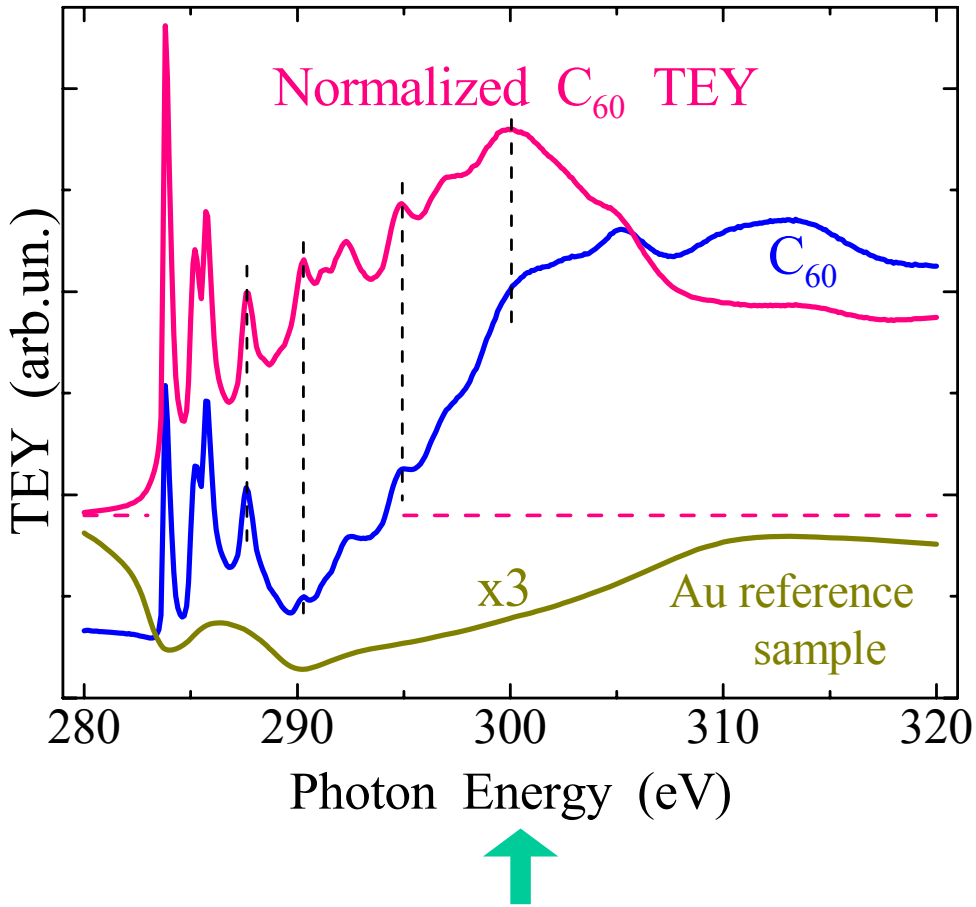

Normalization TEY of C_{60} film using clean Au reference sample

Analysis and Interpretation of NEXAFS Spectra

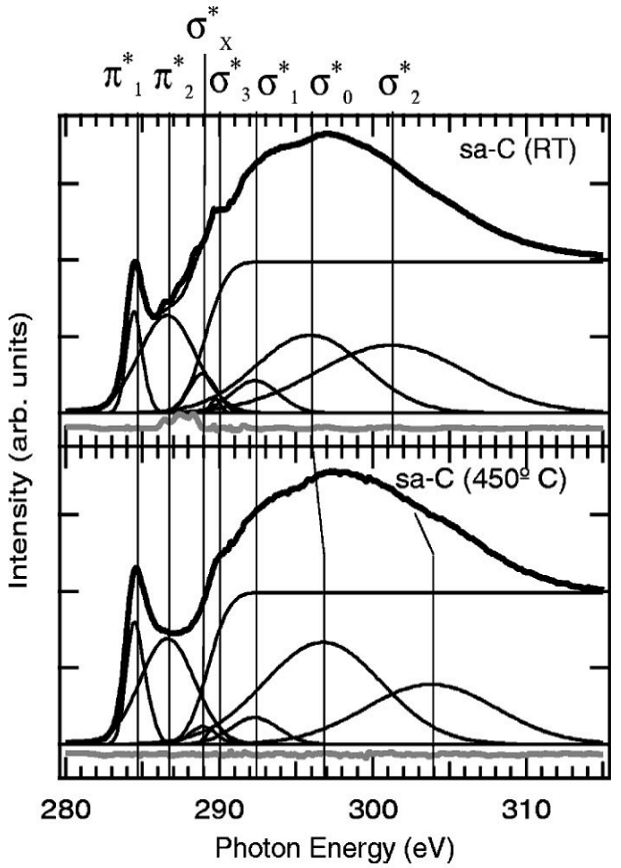

Complicated Way

decomposition into set of steps and peaks, theoretical modeling, etc... [*]

Simplified Way

direct comparison with properly normalized reference spectra

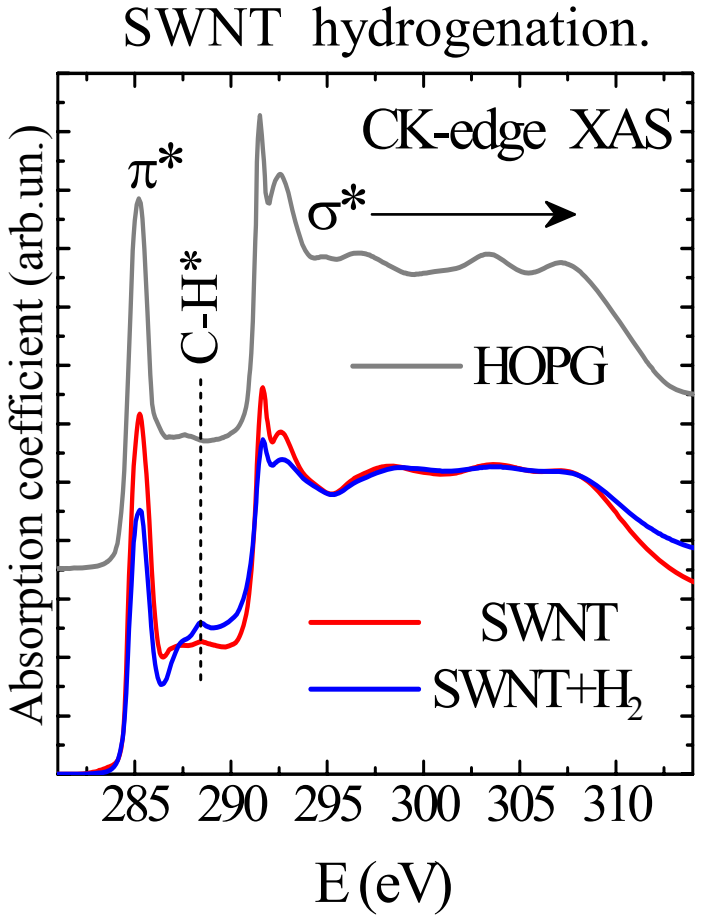

The figure reproduced from J. Diaz, S. Anders, X. Zhou et al. Phys. Rev. B **64**, 125204 (2001).

$$\frac{\pi^*(\mathrm{SWNT}+\mathrm{H_2})}{\pi^*(\mathrm{SWNT})} = 0.72 \pm 0.07$$

[*] For details see references [1- 4] from Main Sources.

IV. The information that can be obtained by NEXAS/EXAFS Spectroscopy. Some Nanocarbons Related Examples

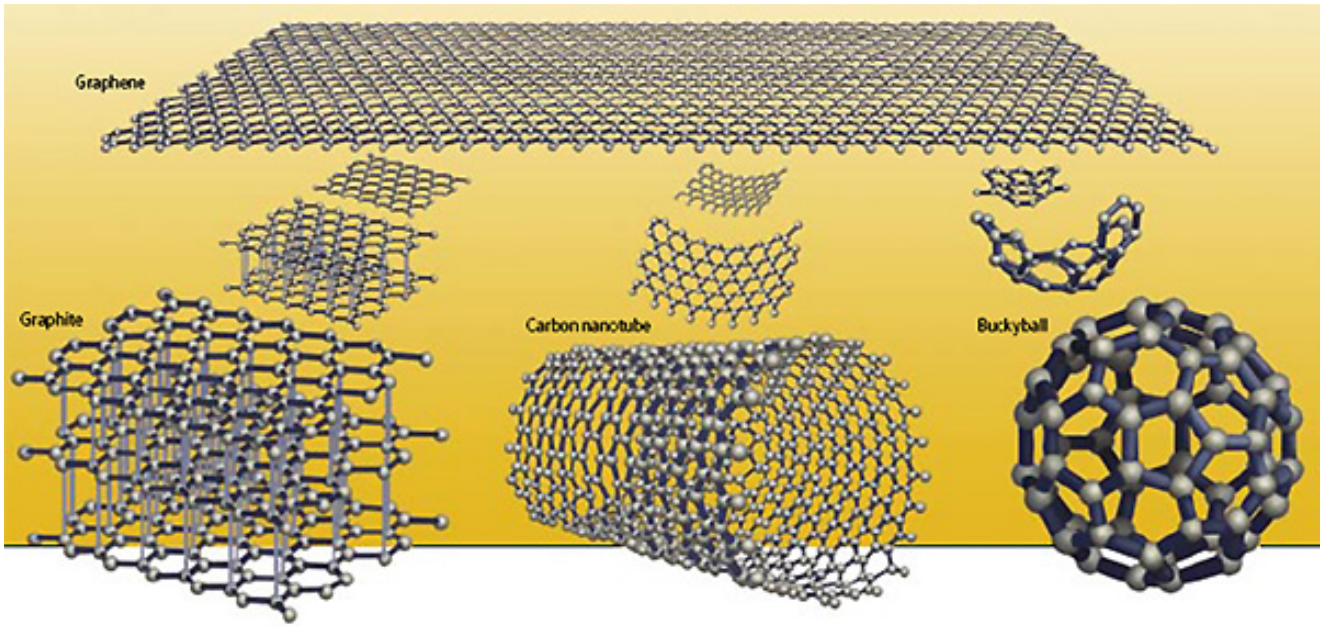

NEXAFS of Fullerites and Fullerides

XAS of C_{60} and C_{60} films [*]

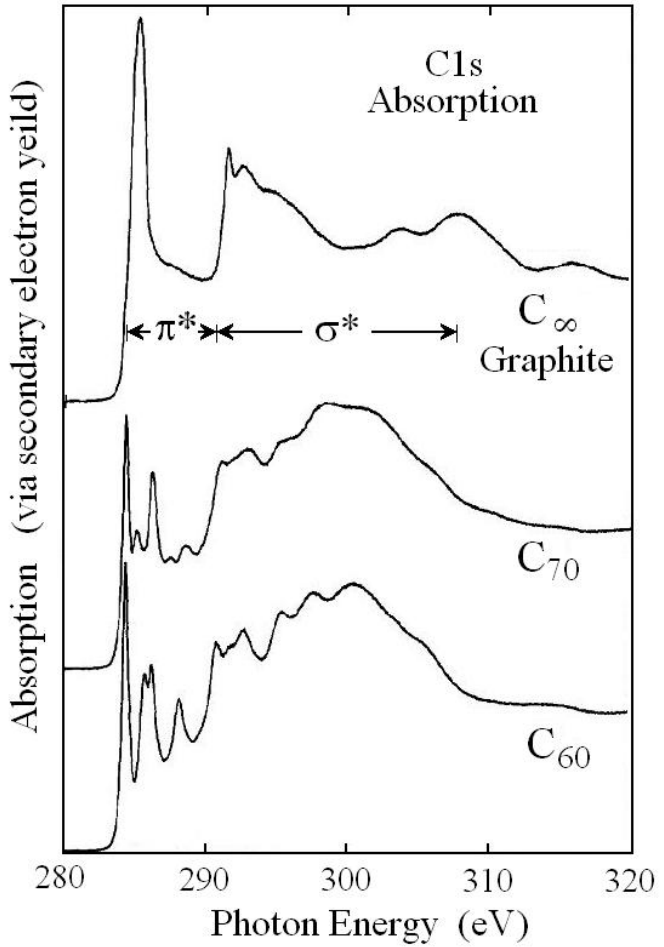

narrow π^* and σ^* resonaces show that solid C_{60} and C_{70} are the molecular crystals

XAS of crystalline K_3C_{60} [**]

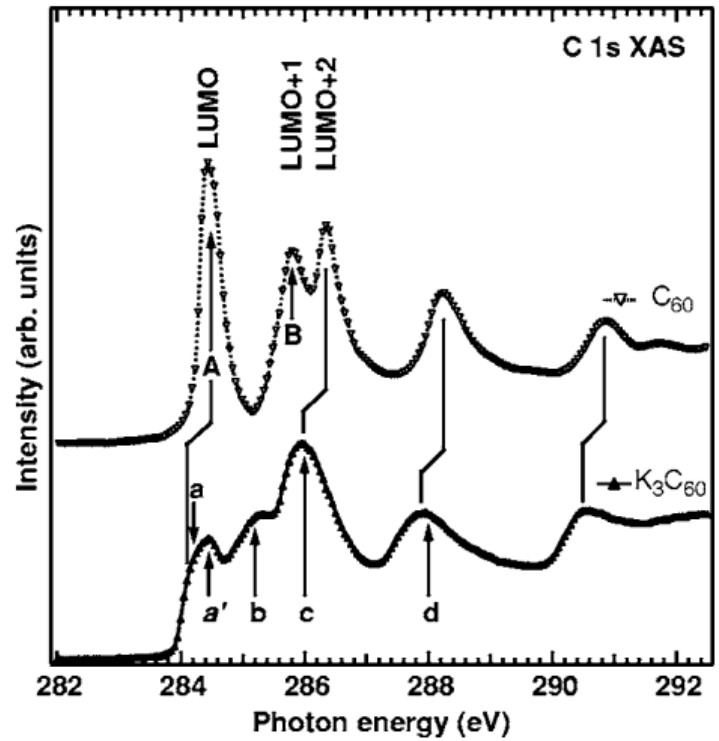

1. half-filled LUMO (a′) in K_3C_{60}.
2. large general shift (~ 0.35 eV) of K_3C_{60} LUMOs

[*] L.J. Termenello et al. Chem. Phys. Letters, **182**, 491 (1991).

[**] T. Kaambre et al. Phys. Rev. B **75**, e195432 (2007).

Experimental and Theoretical study NEXAFS of $C_{60}F_{36}$ [*]

The structure of $C_{60}F_{36}$ isomers

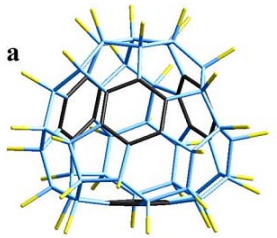

T-symmetry (65%)

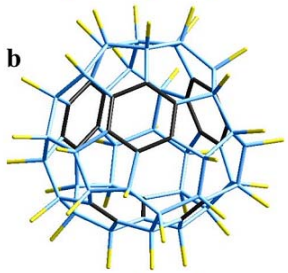

C_1-symmetry (30%)

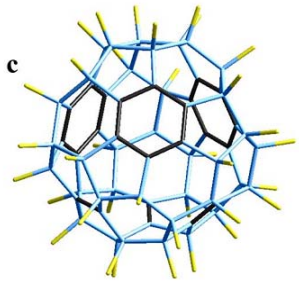

C_3-symmetry (5%)

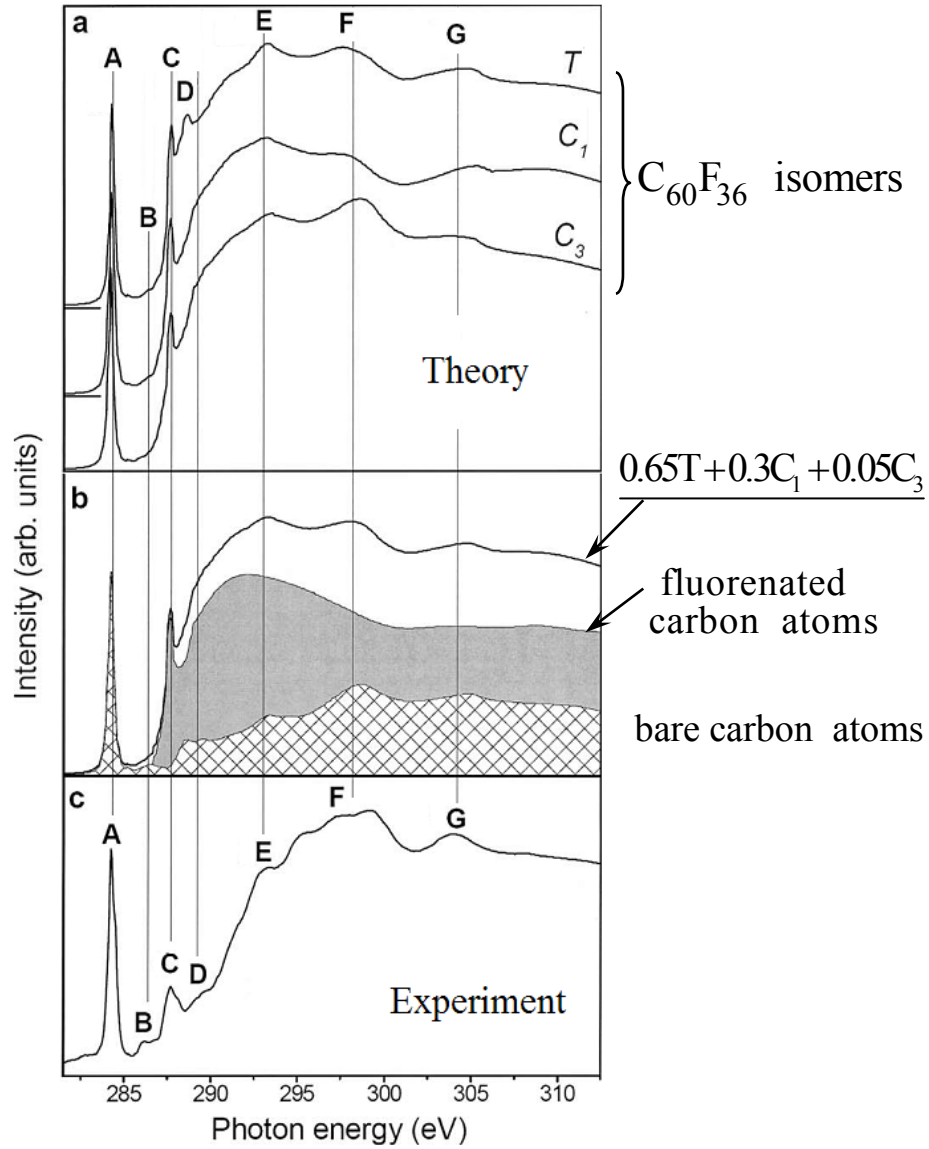

[*] L.G. Bulusheva, A.V. Okotrub, V.V. Shnitov, V. V. Bryzgalov et al. J. Chem. Phys. **130** , 014704 (2009).

NEXAFS of fluorinated MWCNT [*]

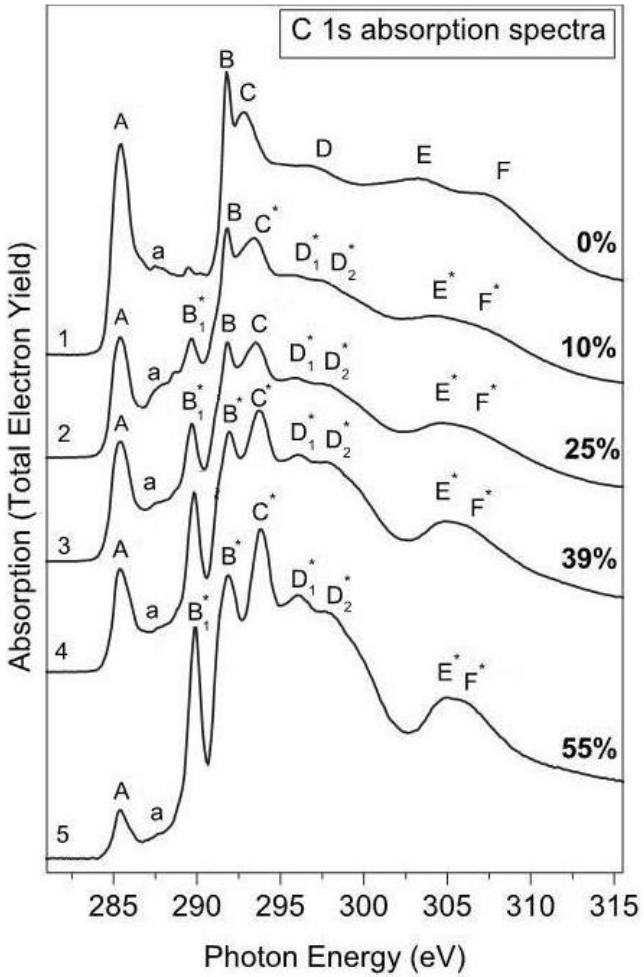

Fluorination dramatically changes MWNT CK-edge, but does not affect their FK-edge

Fluorination "kills" π^*- resonances

$\downarrow$

$sp^2 \rightarrow sp^3$

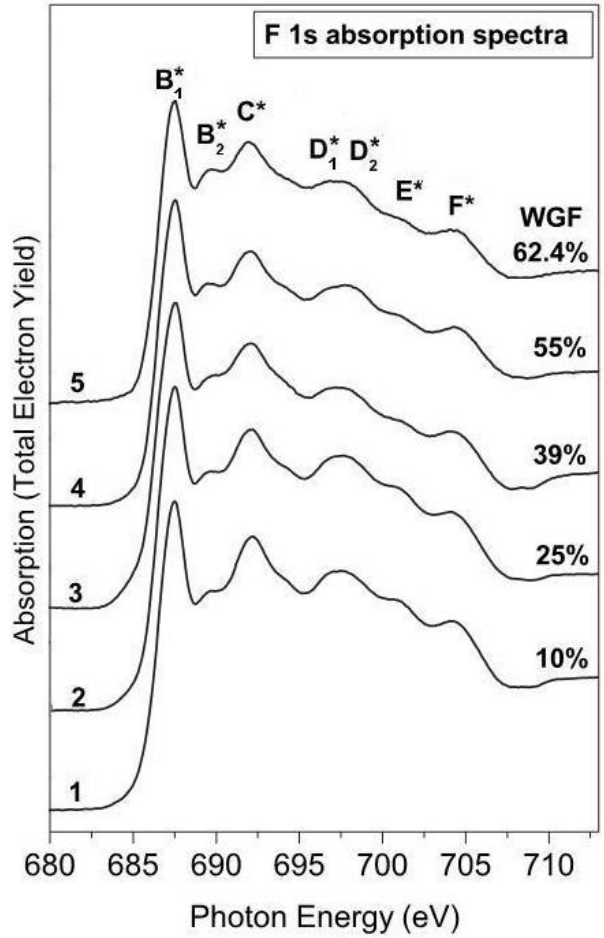

[*] M. M. Brzhezinskaya et al. Phys. Rev. B **79,** 155439 (2009) .

Study of metallicity-sorted SWCNT [*]

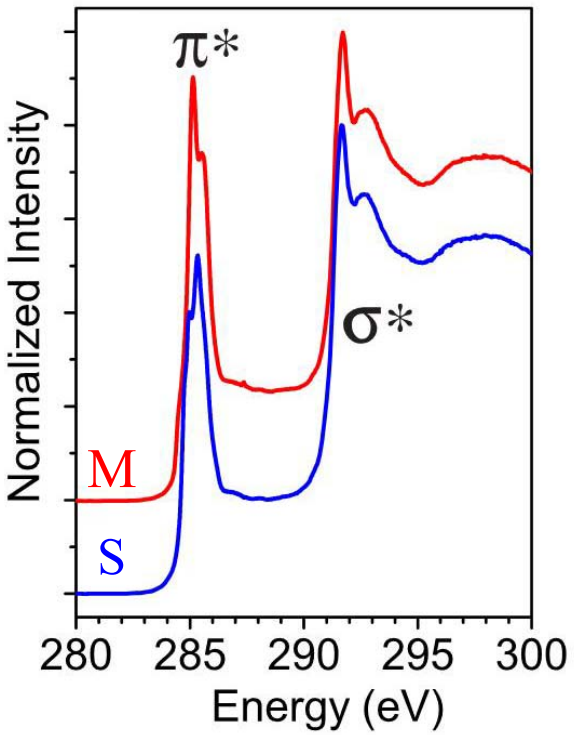

XAS of metallic (M) and semiconducting (S) SWCNTs

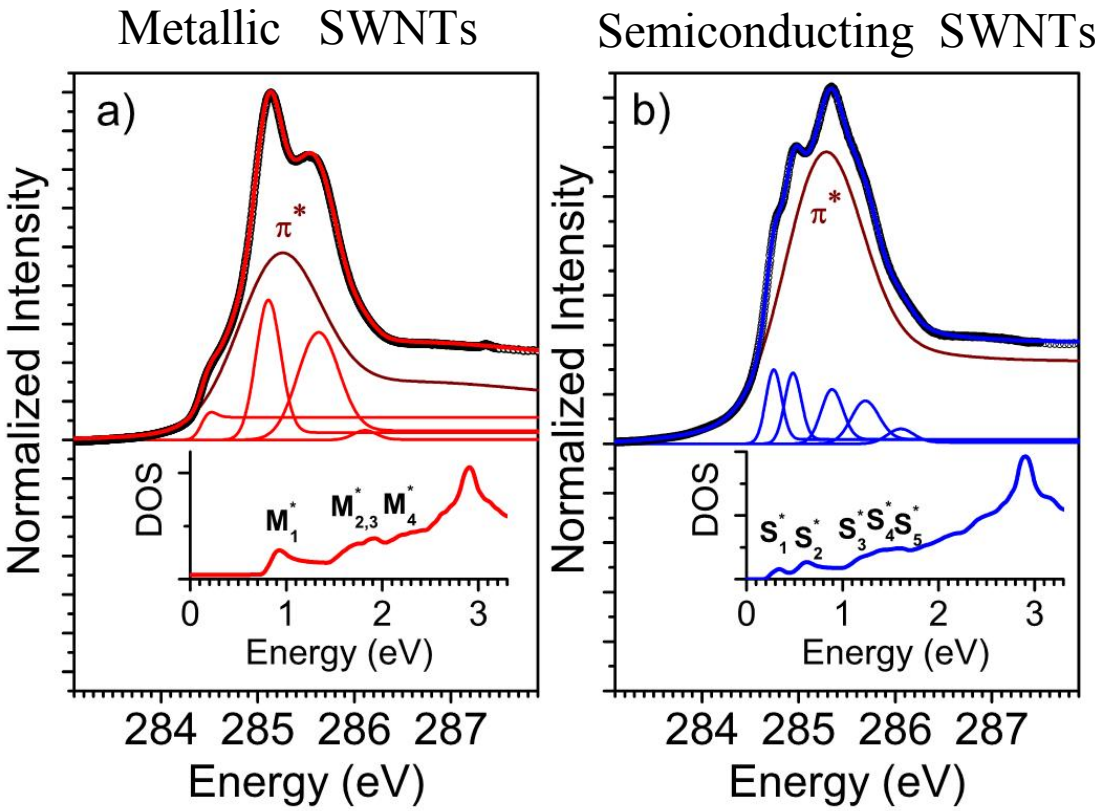

High-resolution XAS C1s absorption edges together with the results of a line shape analysis (thin lines) and TB DOS broadened by the experimental resolution.

[*] P. Ayala et al. Phys. Rev. B **80,** 205427 (2009).

CK-edge NEXAFS of Few Layer Graphene (FGL) [*]

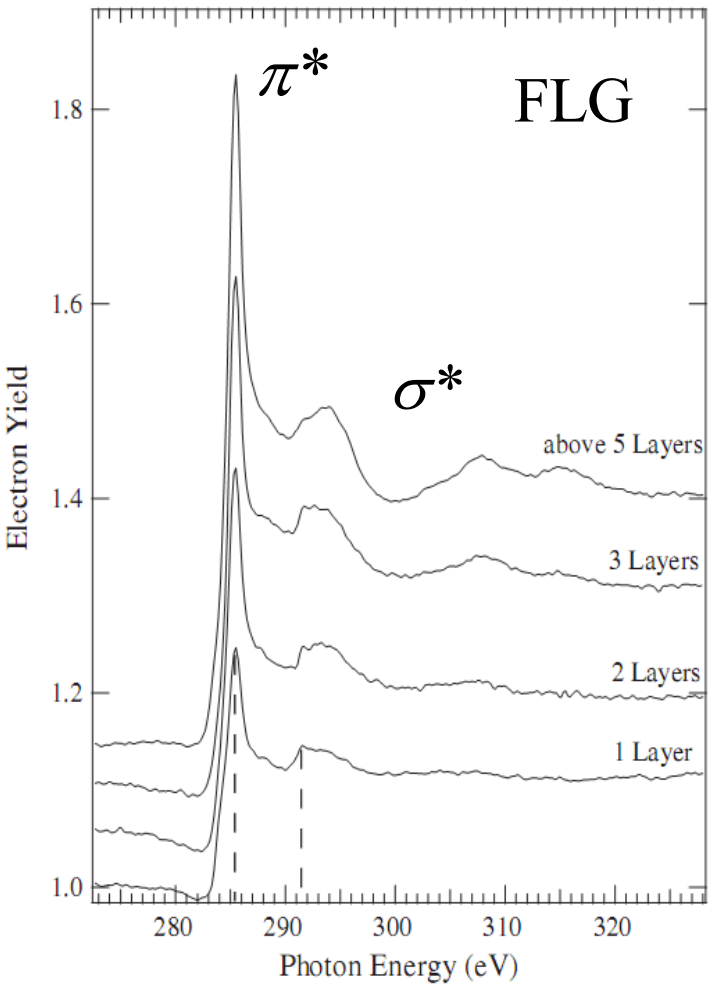

NEXAFS makes possible to distinguish between graphenes with different number of layers

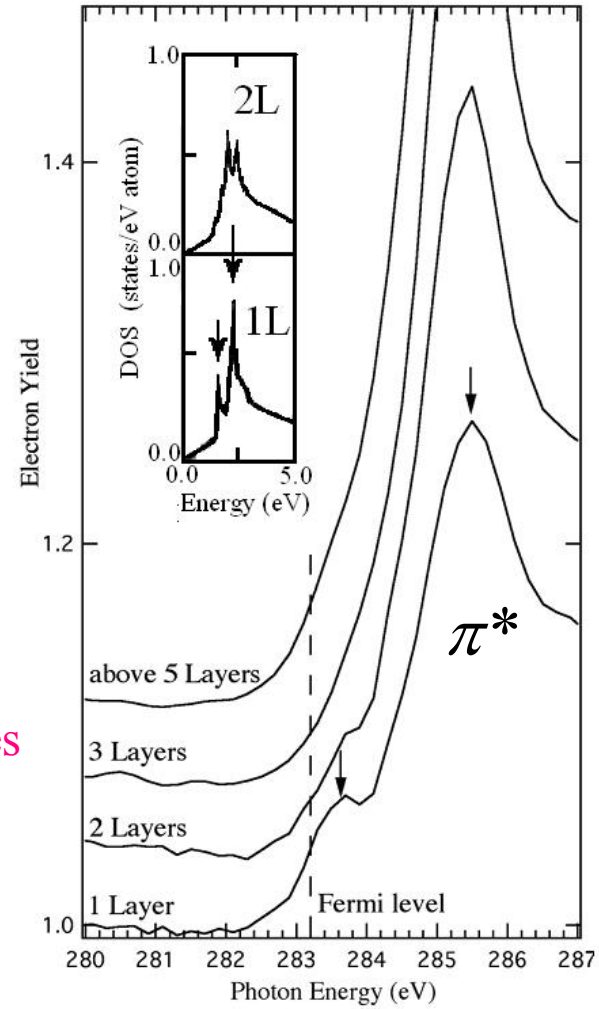

[*] D. Pacile et al., Phys. Rev. Lett. **101,** 066806 (2008) .

NEXAFS study of FLG Grown on 6H-SiC(0001) [*]

CK-edge NEXAFS spectra measured at different incident angles

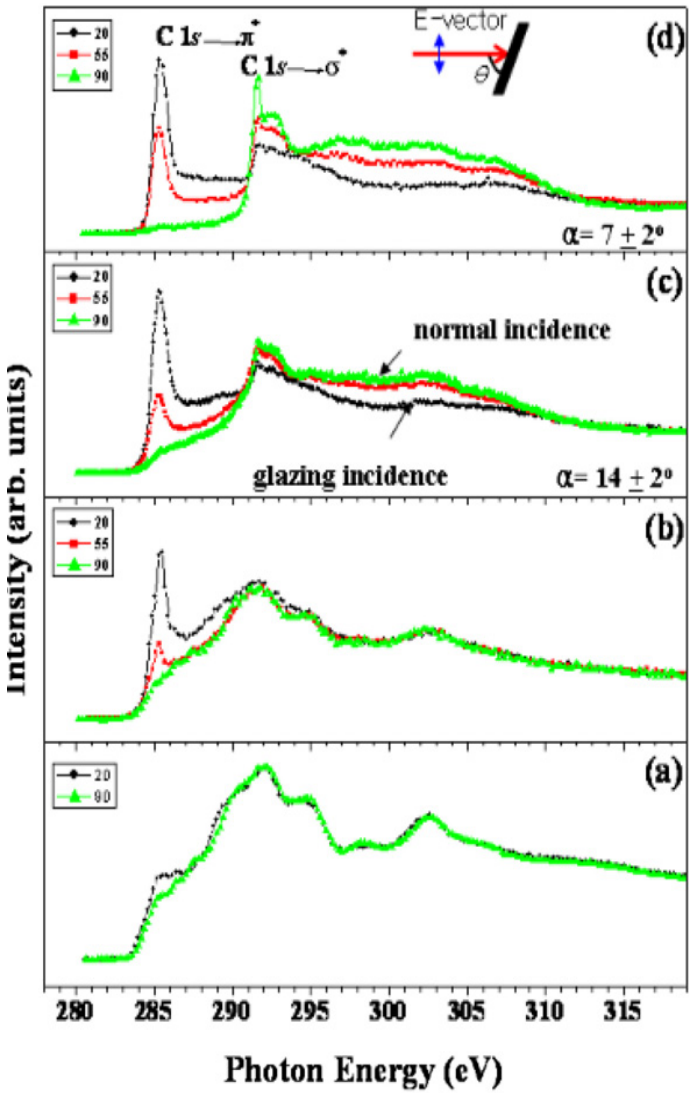

4th annealing at T=1400°C
(formation of thick graphene layer)

3rd annealing at T=1180°C
(growth of single phase graphene layers)

2nd annealing at T=1080°C
(formation of mixed phase (buffer) layer)

1st annealing at T= 900°C
(for substrate outgasing).

[*]. Ki-jeong Kim. J. Phys.: Condens. Matter 20, 225017 (2008).

EXAFS study of I-doped SWNTs [*]

EXAFS experiment at the ESRF (France)

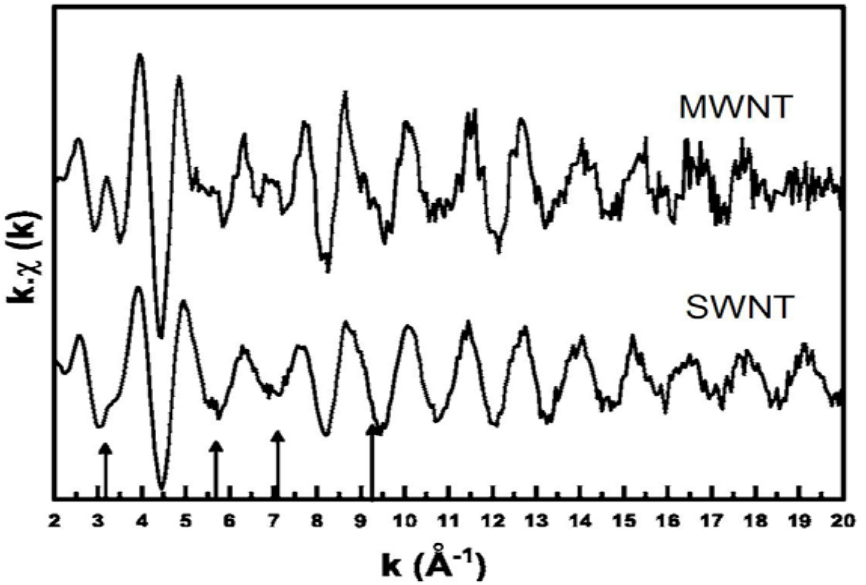

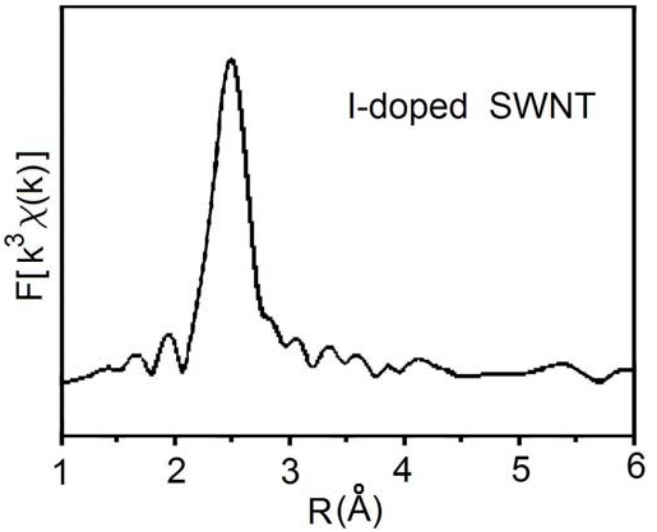

FEFF calculation

Measurements made:

in the transmission mode
at the iodine K - edge (E_o=33.169 keV)
at low temperature (T=10 K)

TABLE 1. Structural parameters deduced from the least square fit of the first shells of the I-doped SWNTs samples

	Iodine shell	Carbon shell
N	0.8	2.2
σ^2	0.0016	0.02
ΔE	12.11	2.8
R	2.74	3.02

[*] T. Michel et al. Phys. Rev. B **73,** 195419 (2006).

V. CONCLUSIONS

1. Modern NEXAFS spectroscopy proved to be one of the most powerful experimental techniques widely used for investigation of nanocarbon materials. It makes possible to probe not only their local electronic structure, but also a chemical composition and even atomic structure.

2. Application of EXAFS spectroscopy in this area of research is much more restricted. As a rule, this technique is used for probing a local atomic structure of composite materials, which along with the carbon atoms contain also the atoms of higher Z elements (such Fe, Ru, I) characterizing by much higher values of absorption edge energy and backscattering amplitude.

VI. MAIN SOURCES:

1. J. Stöhr. NEXAFS spectroscopy. Springer, 1996.

2. M. Newville. Fundamentals of XAFS. University of Chicago, 2004.

3. J. J. Rehr, R. C. Albers. Theoretical approaches to x-ray absorption fine structure. Reviews of Modern Physics, **72**, 621 (2000).

4. X-ray Absorption: Principles, Applications, Techniques of EXAFS, SEXAFS, and XANES, in Chemical Analysis, D. C. Koningsberger and R. Prins, ed., John. Wiley & Sons, 1988.

5. F.W. Lytle. The EXAFS family tree: a personal history of the development of extended X-ray absorption fine structure. J. Synchrotron Rad. **6**, 123 (1999).

Interior view of Synchrotron BESSY II

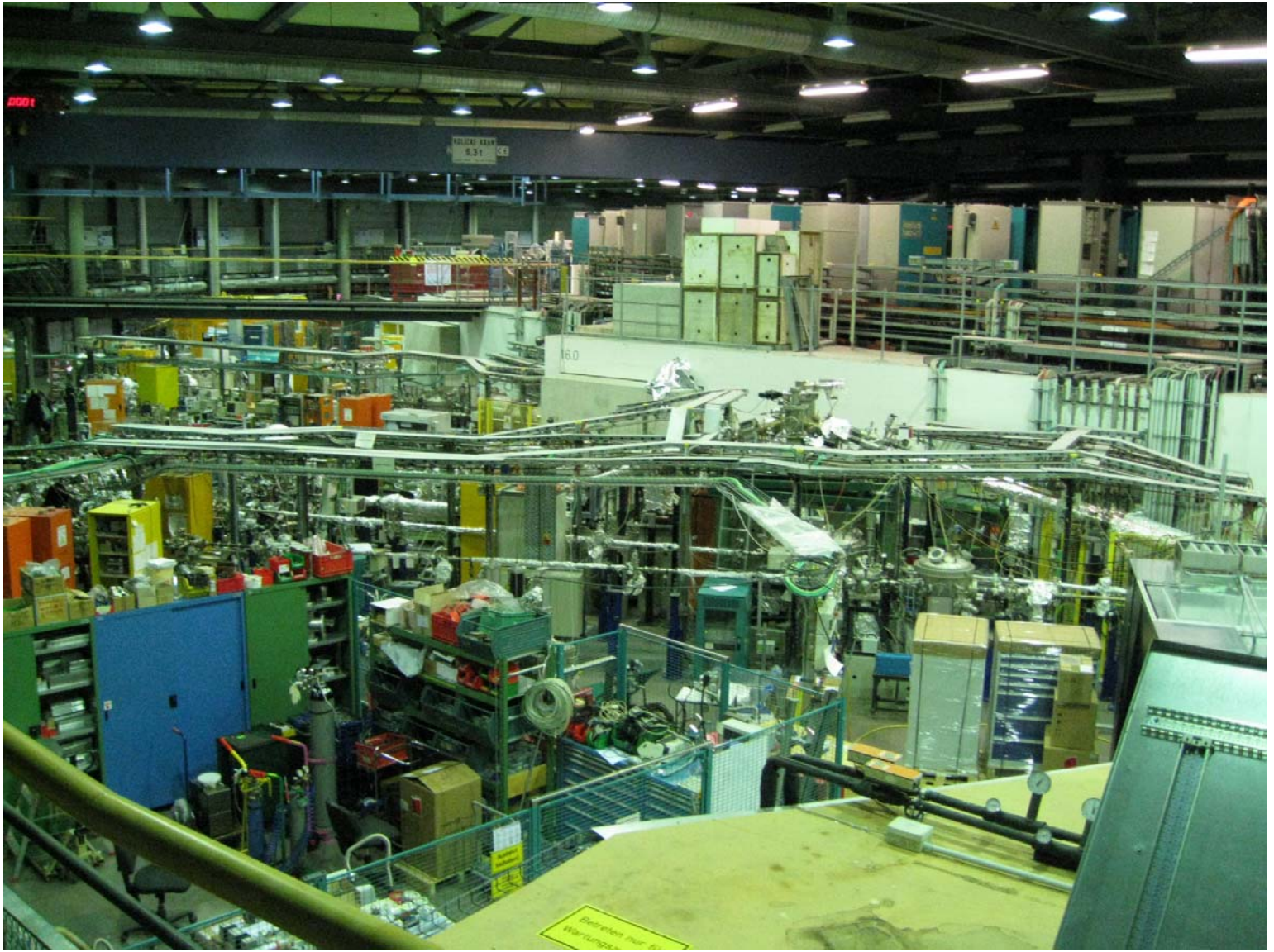

Experimental Station of Russian-German Beam Line